JOURNAL OF MATERIALS SCIENCE 16 (1981) 1257–1263

On the dispersion hardening potential of interphase precipitation in micro-alloyed niobium steel

R. M. BRITO,* H. -J. KESTENBACH†
Instituto Militar de Engenharia, Rio de Janeiro, Brazil

In an experimental high-strength bw-alloy (HSLA) steel micro-alloyed with 0.13 wt% Nb, microhardness of the ferrite phase has been measured as a function of the particle spacing across interphase precipation sheets of niobium carbonitrides. The dispersion geometry was controlled by isothermal transformation treatments using different temperatures and time intervals, and evaluated quantitatively by dark-field transmission electron microscopy. The results were in reasonable agreement with the Orowan–Ashby model of dispersion hardening, suggesting that the sheet spacing may represent the effective geometrical parameter responsible for dispersion hardening due to interphase precipitation.

1. Introduction

Interphase precipitation has been identified as a common precipitation mode for carbonitride particles in micro-alloyed steel where rapid precipitation accompanies the moving γ–α interphase boundary during the austenite-to-ferrite transformation [1–3]. As a result, particles are distributed in a sheet-like array characterized by a more or less regular spacing between individual sheets, which is dependent on transformation temperature, and by a random precipitate arrangement within the sheets [4]. Alternative modes of carbonitride precipitation occur when particles nucleate either in austenite before or in ferrite after the passage of the γ–α interface. In terms of its dispersion hardening potential, interphase precipitation is rated above precipitation in austenite, but below precipitation from supersaturated ferrite [3, 5, 6]. The effect of precipitate strengthening on the mechanical properties of micro-alloyed steel must be controlled very carefully because an increase in yield strength is invariably accompanied by a reduction in toughness.

In structure property relationships [7], the contribution of a fine precipitate distribution to alloy strength is usually derived from the Orowan–Ashby model [8] of dispersion hardening. By measuring the total volume fraction of precipitate and the average particle spacing in a variety of commercial microalloyed steels, Gladman *et al.* [9] have shown that this model can satisfactorily account for the observed increase in yield strength. Strictly, the Orowan–Ashby model has been derived for an average particle spacing in a given slip plane which for a random particle distribution can be replaced by the average spacing measured from a randomly chosen plane of observation.

In the case of interphase precipitation, such an average spacing is difficult to define because, besides the average spacing of the random particle distribution within the individual sheets there exists a more or less regular, and not necessarily related, spacing between particles of adjacent sheets. It could be argued that, in a statistically sufficient number of transmission electron microscopy observations, a truly average particle spacing could be determined which would represent a mean value of the two types of spacings defined above. However, due to the large number of possible slip planes and profuse cross-slip commonly observed in ferrite samples, and due to the random orientation of precipitate sheets which is not related to

*Present address: Companhia Siderúrgica Nacional, Volta Redonda, Rio de Janeiro, Brazil.
†Present address: Departamento de Engenharia de Materiais, Universidade Federal Se São Carlos, São Carlos, S.P. Brazil.

0022–2461/81/051257–07$02.70/0

TABLE I Chemical compositions of the micro-alloyed steels

Alloy	Elements content (wt %)								
	C	Mn	P	S	Si	Cu	Cr	Al	Nb
1	0.17	1.33	0.022	0.021	0.25	0.22	0.46	0.03	0.03
2	0.15	1.30	0.021	0.022	0.23	0.22	0.49	0.03	0.13

slip geometry, it must be expected that dislocations are able to select those slip planes in which they encounter particle spacings which are larger than the statistical mean.

From transmission electron microscopy observations, a separate measurement of the average particle spacing within a precipitation sheet could only be attempted when the sheet lay nearly parallel to the foil plane. Due to the random sheet orientation, such a condition is difficult to control. On the other hand, it is a relatively simple task to measure the average spacing between individual sheets in orientations where the sheets lie approximately parallel to the electron beam. In fact these are the only orientations in which interphase precipitation can be recognized from the particle morphology alone [6], for the case of small inter-sheet spacings (small with respect to the foil thickness).

During the course of an isothermal transformation study on a high Nb-content micro-alloyed steel, interphase precipitation was found to be associated with a relatively large increase in ferrite microhardness, probably due to a large degree of supersaturation obtained through quenching from a high solution temperature into a salt bath. Maximum hardness values were found to be equivalent to an increase of 400 MPa in yield strength, while the contribution of precipitation strengthening in commercial niobium micro-alloyed steel is usually estimated to be around 100 MPa [6, 10]. In view of the discussion on average and effective particle spacings presented above, it was considered worthwhile to analyse the effect of experimentally observed interphase precipitation sheet spacing on measured ferrite hardnes values through the Orowan–Ashby model.

2. Experimental procedures

Table I shows the chemical composition of the experimental hot-rolled 0.13 wt% Nb alloy, together with that of a commercial 0.03 wt % Nb steel. Both steels were subjected to identical heat treatments in order to study the effect of a high Nb-content on the precipitation hardening potential of micro-alloyed steel. The material was solution treated at 1250° C for 2 h under vacuum, oil quenched and re-austenized at the same temperature for 15 min in order to reduce austenite grain growth. At the end of the second austenite holding period, different samples were isothermally transformed in salt baths at temperatures ranging from 600 to 700° C during time intervals of between 5 and 60 min and finally water quenched to room temperature. Salt bath temperatures were controlled to within ± 5° C. Metallographic specimens were etched in 2 vol% Nital or in a solution containing 98 vol % H_2O_2 (30%), 1 vol % HF and 1 vol % HBF_4. Ferrite micro-hardness values were measured with loads of 15 g and 50 g. Mean hardness values for each sample were determined from 10 individual random measurements. Comparing hardness values taken from the same sample, it was found that a 15 g load led consistently to higher hardness values than a 50 g load. Therefore, hardness values for small ferrite grains (in samples of small transformed volume fractions), which could only be measured under a 15 g load, were corrected using the following expression determined empirically for the correlation between hardness values, H_{V50} and H_{V15}, taken with loads of 50 g and 15 g, respectively:

$$H_{V50} = 3.1\,(H_{V15})^{0.788} \qquad (1)$$

Samples for investigation using transmission electron microscopy (TEM) were prepared by the window technique, initially employing a chemical solution of 92 wt % of H_2O_2 (30%) and 8 vol % of HF, at room temperature, while final thinning was conducted electrolytically in a solution of 1 vol % $HClO_3$ in CH_3OH at 40 V and − 60° C. All electron microscope observations were performed on samples of the high Nb-content steel. Spacings between interphase precipitation sheets were measured in suitably orientated foil areas. Mean particle diameters were determined by direct measurements on high magnification dark-field micrographs.

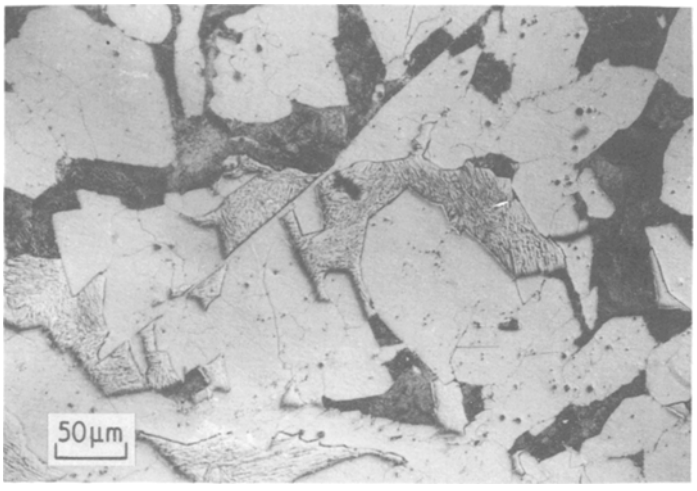

Figure 1 Ferrite, pearlite (dark areas) and acicular microconstituents (grey areas) in a sample partially transformed at 650° C for 30 min.

3. Results

After the isothermal transformation treatments, followed by water quenching, the phases present in both steel compositions were ferrite, pearlite and acicular microconstituents in regions where the remaining austenite had transformed during the water quench, see Fig. 1. With smaller transformed volume fractions of ferrite the prior austenite grain size could be determined, see Fig. 2, giving a mean grain diameter of 220 μm for the 0.13 wt % Nb alloy and 410 μm for the 0.03 wt % Nb steel.

In Fig. 3, the ferrite hardness is plotted as a function of transformation temperature; for any given temperature, only the range of hardness values encountered is indicated. There was no consistent change of ferrite hardness with isothermal holding time, possibly due to the fact that niobium carbonitrides form relatively stable dispersions at these temperatures [11] with little change after the nucleation and initial growth events in the interphase boundary. However, the greater hardening potential of the high Nb-content steel at lower transformation temperatures is clearly evident from Fig. 3.

Because of the low transformed volume fractions of ferrite at 600° C (less than 20%), only those samples treated at 650, 675 and 700° C were analysed by transmission electron microscopy.* Fig. 4 shows typical bright-field and dark-field examples of the interphase precipitation mode which were found in all the samples observed. Quantitative measurements of particle size and spacings between precipitation sheets are presented

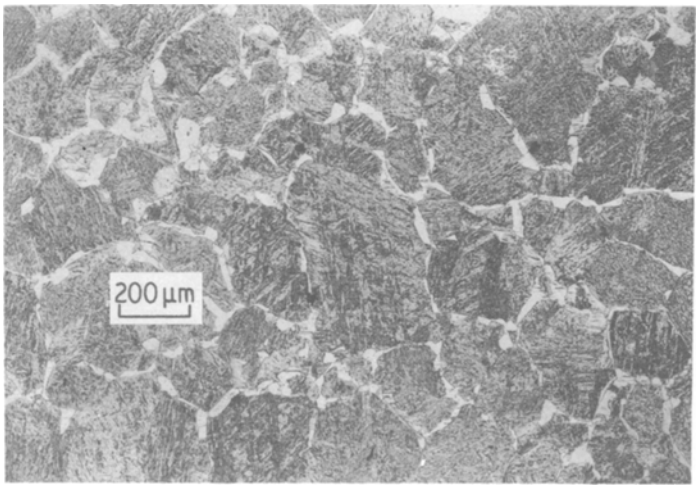

Figure 2 Ferrite outlining the austenite grain boundaries in a sample partially transformed at 700° C for 10 min.

*The reason for this is the lengthy procedure of electron beam alignment required during a specimen tilt of ferromagnetic foils; excessive foil contamination during such tilts made it necessary to scan rapidly large sample areas in order to find interphase precipitation sheets suitably orientated for spacing measurements.

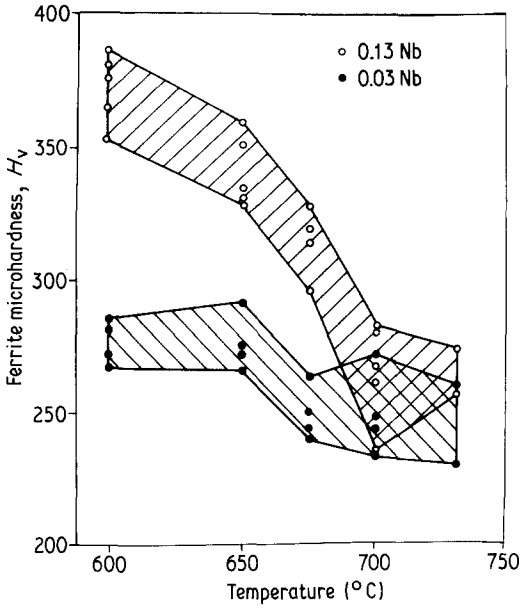

Figure 3 Vickers microhardness of ferrite as a function of isothermal transformation temperature for high and low niobium-content steels.

in Table II, together with the microhardness values obtained from the respective metallographic samples. The last column of Table II gives the increments in yield strength, $\Delta\tau$, calculated from [9],

$$\Delta\tau = \frac{1}{1.18}\frac{1.2Gb}{2\pi L}\ln\frac{\bar{X}}{2b}, \quad (2)$$

where G is the shear modulus (80 300 MPa for ferrite), b is the magnitude of the Burgers vector (0.25 nm for ferrite), L is the free spacing between particles and $\bar{X}$ is the mean effective particle diameter in the slip plane. The average spacings between precipitation sheets were used for L. The mean effective particle diameters $\bar{X}$ listed in Table II were determined from the measured average particle diameters $\bar{D}$, according to [9]:

$$\bar{X} = \bar{D}(\tfrac{2}{3})^{1/2}. \quad (3)$$

In Fig. 5, measured ferrite microhardness, H_V, has been plotted as a function of the yield strength increment, $\Delta\tau$, predicted from Equation 2 and based upon the observed interphase precipitation geometry. Least-square fit analysis showed that the data could be represented by a best-fit straight line

$$H_V = 148 + 0.548\Delta\tau \quad (4)$$

with a correlation coefficient $r^2 = 0.82$. It can be seen from Fig. 5 that the calculated increment of yield strength reaches 400 MPa. This increment is

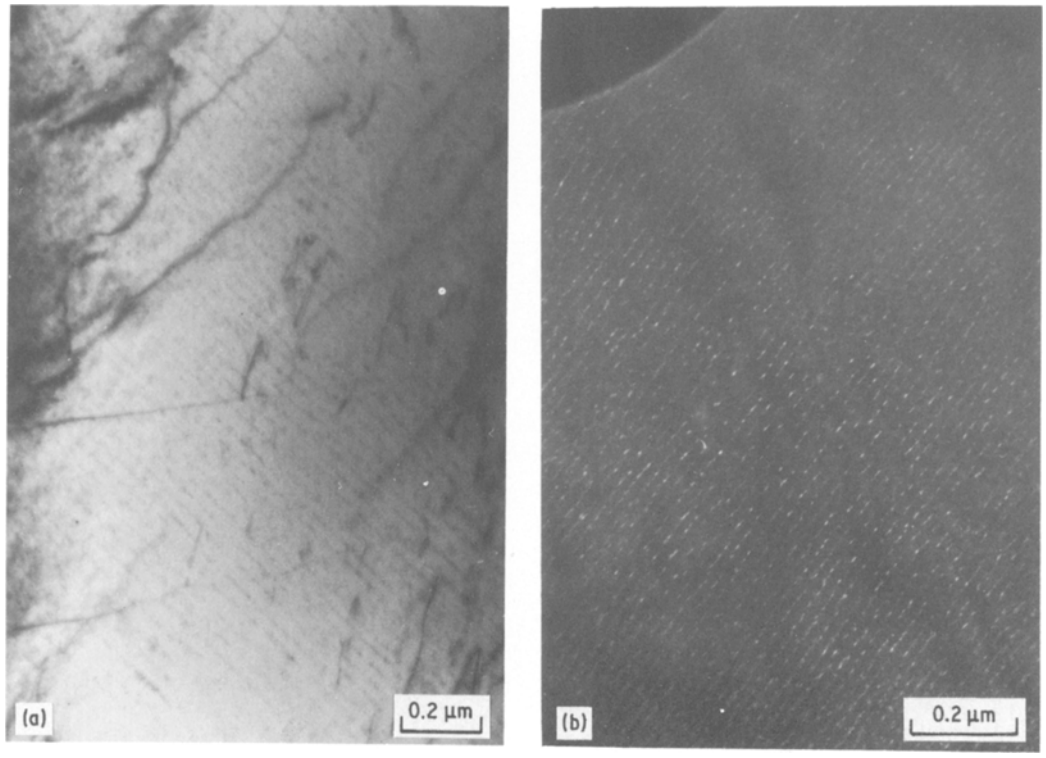

Figure 4 Typical bright-field and dark-field electron micrographs of the interphase precipitation. Transformation temperatures (a) 675° C and (b) 650° C.

TABLE II Particle size and sheet spacings for interphase precipitation with resulting microhardness and yield strength increments

Sample	Isothermal transformation		Corrected particle diameter (Å)	Sheet spacing (Å)	Microhardness, H_V	Calculated yield strength increase, $\Delta\tau$ (MPa)
	Temperature (° C)	Time (min)				
A8	700	50	41	340	268	201
A16	700	60	49	335	236	221
A26	675	40	62	270	313	303
A27	675	60	47	268	313	272
A13	650	30	49	190	349	390
A11	650	40	33	160	358	383
A14	650	60	38	220	332	299

associated with the higher microhardness values measured in samples transformed at 650° C (compare with values in Fig. 3). The significance of Fig. 5 will be further discussed below.

In principle, the observed dispersion strengthening could have been caused by other carbonitride precipitation modes. Extensive electron diffraction analysis was performed in order to identify the orientation relationships between the carbonitride precipitates and the ferrite which will indicate whether nucleation had occurred in austenite, γ–α interface or in ferrite [6]. Clear evidence could only be obtained for austenite precipitation where, in the absence of austenite deformation and recrystallization, a single but random particle orientation with respect to the ferrite has been reported in the literature [6]. The relatively small number and frequent alignment of individual particles in these cases suggested that nucleation had occurred preferentially on austenite dislocations introduced by quenching stresses, see Fig. 6.

In ferrite, both interphase precipitation and nucleation are reported to occur according to the Baker–Nutting relationship: $(1\,0\,0)_{NbC} \parallel (1\,0\,0)_\alpha$ and $[0\,1\,1]_{NbC} \parallel [0\,1\,0]_\alpha$. Precipitation in ferrite is expected to occur at random with any one of the three possible variants described by this relationship, whereas a preferred nucleation effect at the γ–α boundary should lead to the presence of only one variant in the case of interphase precipitation [4]. In the present work, two different particle orientations were observed in several samples and foil regions characterized by relatively

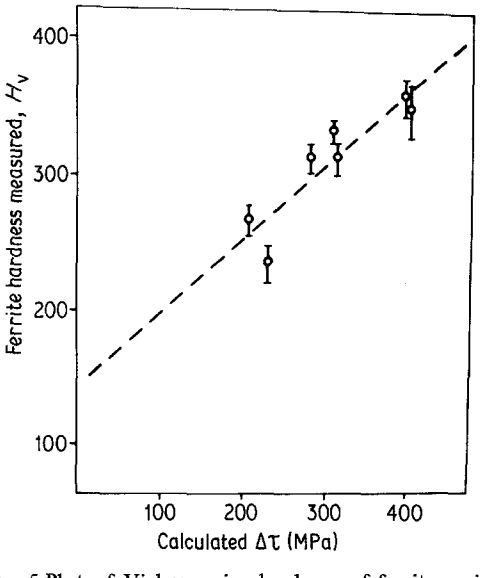

Figure 5 Plot of Vickers microhardness of ferrite against yield strength increment calculated from the Orowan–Ashby model.

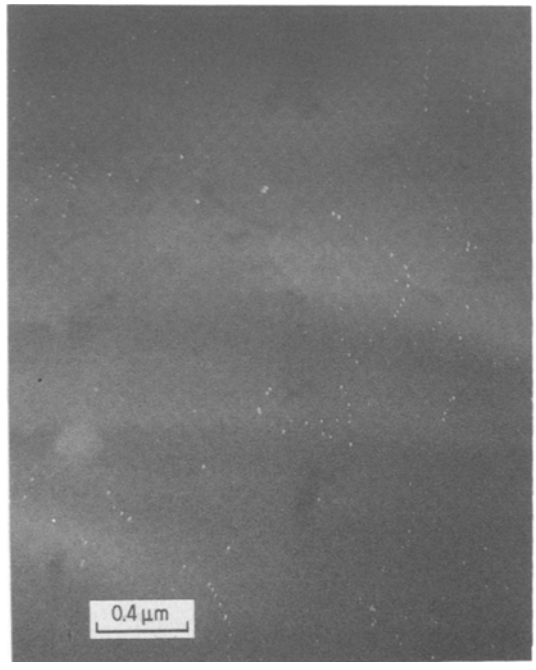

Figure 6 Precipitation of Nb(C, N) in austenite at 675° C before the start of transformation.

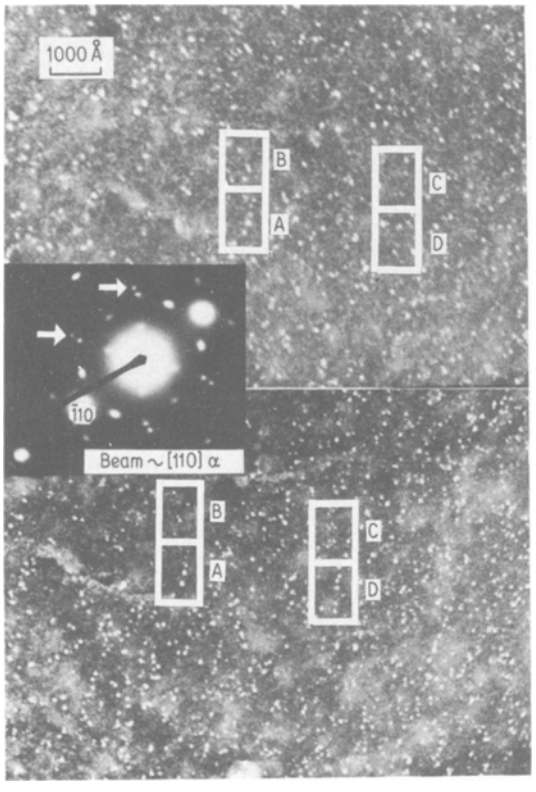

Figure 7 Precipitation of Nb(C, N) at 700° C in two dark-field micrographs. Particles at A belong to both Nb(C, N) reflections arrowed in the diffraction pattern and were probably nucleated in austenite. Most of the other particles, for example B, C and D, are associated with only one of the two Nb(C, N) reflections. Other second-phase reflections are oxide spots. See text for discussion.

dense precipitate distributions. A particularly interesting example is shown in Fig. 7 where two Nb(C, N) reflections are present in the diffraction pattern. For the given ferrite orientation neither one of the reflections agrees with the Baker–Nutting relationship while both reflections could be associated with nucleation from a single but random austenite orientation. However, careful comparison of the two dark-field micrographs revealed that only a few particles were associated with both reflections (for example at A) whereas most of the particles (for example at B, C and D) belonged to only one of the two reflections. Thus, the majority of the particles shown in Fig. 7 exhibit an orientation which does not agree with the established orientation relationships of any of the three precipitation modes. It appears likely, however, that these particles in Fig. 7, and others observed in similar distributions with "unconventional" orientation relationships, have originated during interphase precipitation as described in the discussion below.

4. Discussion

It is well known that the supersaturation of the matrix with respect to niobium carbonitride increases abruptly when the steel transforms from austenite to ferrite. At a constant temperature, precipitation in austenite should therefore always lead to a smaller number of particles per unit volume in comparison with either interphase precipitation or post-transformation nucleation in ferrite. This argument is confirmed by the type of particle distribution shown in Fig. 6. It is clear that, in this case, the strengthening contribution from precipitation in austenite must be comparatively small.

As judged from electron diffraction evidence the "unconventional" precipitate orientations referred to above may also have been generated by nucleation in ferrite as well as by interphase precipitation. In the absence of definite experimental proof, the authors have ruled out the hypothesis of nucleation in ferrite for the following reasons.

Firstly, the presence of the γ–α boundary during interphase precipitation should lead to a smaller critical size for the precipitate nucleus. Therefore, as long as both reactions occur at the same temperature, nucleation in ferrite after the passage of the α–γ interface should be associated with a smaller number of particles per unit volume. However, particle densities observed in areas such as that shown in Fig. 7 were not very different from particle densities found in other regions where "conventional" precipitate orientations could unambiguously be identified with interphase precipitation.

Secondly, there exists a simple argument [3] for the growth of different orientations in the γ–α interface: due to the fcc structure of Nb(C, N), nucleation is more likely to occur on the austenite side of the boundary. Unexpected orientations may however be preferred since particle growth should proceed preferentially in the ferrite because of a larger supersaturation and because of faster diffusion rates.

It thus appears safe to assume that interphase precipitation has been responsible for the high ferrite hardness, observed in Fig. 3, for lower transformation temperatures. The data presented in Fig. 5 will now be analysed in order to show

that the average spacing between interphase precipitation sheets appears to act as the effective barrier to dislocation motion and therefore controls the degree of dispersion hardening. In order to verify this, it is necessary to compare Equation 4 with established relationships between hardness and yield strength.

For Vickers hardness measurements, the following expression has been proposed [13]:

$$\sigma_y = \frac{H_V}{3}(0.1)^{m-2}, \quad (5)$$

where σ_y is the tensile yield stress, in kg mm^{-2}, H_V is the Vickers hardness number and m is the Meyer's hardness exponent which in materials with high hardness values has a value close to 2 [13]. Substituting $m = 2$ and $\tau_y = 0.5\sigma_y$ for the maximum resolved shear stress into Equation 5 yields

$$H_V = 0.612\tau_y, \quad (6)$$

where τ_y is now expressed in MPa. Considering the various approximations used in this analysis, the value of the constant, of 0.612, compares favorably with the coefficient of 0.548 determined experimentally in Equation 4 which converts the calculated yield strength increment due to inter-sheet precipitation strengthening into a measured microhardness. In addition, the value of $148H_V$ predicted by Equation 4 for $\Delta\tau = 0$ appears to be a reasonable ferrite microhardness for the mild steel of present composition in the absence of precipitation hardening [14].

According to solubility data, in [15], 0.077 wt% Nb could be dissolved in the high Nb-content steel at 1250° C. Usually, total niobium additions to commercial micro-alloyed steels are smaller than this amount. Furthermore, precipitation in austenite during hot rolling will further reduce the amount of Nb left in solution at the transformation temperature. The large yield strength increments in the range of 400 MPa can therefore simply be explained by a high degree of supersaturation which does generally not exist in commercial Nb micro-alloyed steel. It is nevertheless interesting to realize that interphase precipitation can occur on a scale fine enough to produce such a large strengthening effect. On the other hand, it may be expected that the transformation kinetics and thus the hardenability of a given steel may exert an important influence on the interphase precipitation sheet spacing and, thereby, on the amount of dispersion hardening.

5. Conclusions

Dispersion hardening in a high Nb-content micro-alloyed steel equivalent to a 400 MPa increment in yield strength has been accounted for by interphase precipitation. An Orowan–Ashby type of analysis suggested that the spacing between precipitate sheets represents the effective barrier to dislocation motion in such a steel.

Acknowledgements

Financial support from the Ministério de Planejamento and the Brazilian Army through the IME Materials Research Centre is gratefully acknowledged. The authors would like to thank the Companhia Siderúrgica Nacional for providing materials and heat-treating facilities. RMB received a scholarship from the National Research Council CNPq during the course of this work.

References

1. W. B. MORRISON, *J. Iron and Steel Inst.* **201** (1963) 317.
2. A. T. DAVENPORT, F. G. BERRY and R. W. K. HONEYCOMBE, *Met. Sci. J.* **2** (1968) 104.
3. J. M. GRAY and R. B. G. YEO, *Trans. ASM* **61** (1968) 255.
4. A. T. DAVENPORT and R. W. K. HONEYCOMBE, *Proc. Roy. Soc.* **A322** (1971) 191.
5. J. M. GRAY, D. WEBSTER and J. H. WOODHEAD, *J. Iron and Steel Inst.* **203** (1965) 812.
6. A. T. DAVENPORT, L. C. BROSSARD and R. E. MINER, *J. Metals* **27** (1975) 21.
7. F.B. PICKERING and T. GLADMAN, Iron and Steel Institute, London, Special Report number 81 (1963) p. 10.
8. M. F. ASHBY, *Acta Met.* **14** (1966) 679.
9. T. GLADMAN, B. HOLMES and I. D. McIVOR, "The Effect of Second Phase Particles on the Mechanical Properties of Steel" (I.S.I., 1971) p. 58.
10. R. W. K. HONEYCOMBE, *Met. Trans. A* **7A** (1976) 915.
11. P. SCHWAAB and G. LANGENSCHEID, *Pract. Metallogr.* **IX** (1972) 67.
12. R. G. BAKER and J. NUTTING, I.S.I. Special Report number 64 (1959) p. 1.
13. J. R. CAHOON, W. H. BROUGHTON and A. R. KUTZAK, *Met. Trans.* **2** (1971) 1979.
14. G. L. DUNLOP, C. J. CARLSSON and G. FRIMODIG, *Met. Trans. A* **9A** (1978) 261.
15. H. NORDBERG and B. ARONSSON, *J. Iron and Steel Inst.* **206** (1968) 1263.

Received 12 August and accepted 22 October 1980.